Published in final edited form as:
Magn Reson Imaging. 2009 October ; 27(8): 1151–1162. doi:10.1016/j.mri.2009.05.003.

On high *b* diffusion imaging in the human brain: ruminations and experimental insights☆

Robert V. Mulkern[a,b], **Steven J. Haker**[b,*], and **Stephan E. Maier**[b]

[a]Department of Radiology, Children's Hospital, Harvard Medical School, Boston, MA 02115, USA

[b]Department of Radiology, Brigham and Women's Hospital, Harvard Medical School, Boston, MA 02115, USA

Abstract

Interest in the manner in which brain tissue signal decays with *b* factor in diffusion imaging schemes has grown in recent years following the observation that the decay curves depart from purely monoexponential decay behavior. Regardless of the model or fitting function proposed for characterizing sufficiently sampled decay curves (vide infra), the departure from monoexponentiality spells increased tissue characterization potential. The degree to which this potential can be harnessed to improve specificity, sensitivity and spatial localization of diseases in brain, and other tissues, largely remains to be explored. Furthermore, the degree to which currently popular diffusion tensor imaging methods, including visually impressive white matter fiber "tractography" results, have almost completely ignored the nonmonoexponential nature of the basic signal decay with *b* factor is worthy of communal introspection. Here we limit our attention to a review of the basic experimental features associated with brain water signal diffusion decay curves as measured over extended *b*-factor ranges, the simple few parameter fitting functions that have been proposed to characterize these decays and the more involved models, e.g.,"ruminations," which have been proposed to account for the nonmonoexponentiality to date.

Keywords

b Factor; Diffusion imaging; Human brain; Ruminations

1. Brain water diffusion decay curves

Countless literature reiterations of the basics of diffusion measurement [1] and/or diffusion imaging with MR [2] mandate, in the interest of the rainforests, only the briefest technical discussion. A diffusion signal decay curve will, for our purposes, consist of the natural logarithm of the MR signal *S*, plotted against the so-called *b* factor, an experimentally controlled parameter which determines the degree of diffusion weighting applied to the object. For the most commonly employed spin-echo diffusion preparation sequences, the *b* factor is defined by the timing and amplitude specifics of the two balanced gradient pulses placed on either side of the refocusing RF pulse. In terms of their amplitude *g*, duration δ and the distance between their leading edges Δ, the *b* factor reads:

☆This work was supported in part by NIH grant 1 R01 EB006867 and U41RR019703.

*Corresponding author. haker@bwh.harvard.edu (S.J. Haker).

$$b=(\gamma g\delta)^2[\Delta-\delta/3] \quad (1)$$

where γ is the gyromagnetic ratio (2π×4258 Hz/Gauss) for protons. The most common units employed for *b* are seconds per square millimeter (1 s/mm^2=10^{-6} s/m^2 in SI units) and the term in brackets is often referred to as the "diffusion time" and loosely reflects a measure of the time over which the diffusion process is being observed. When restrictions to diffusion occur, such as from cellular membranes, etc., the diffusion time becomes an important consideration. Of course, the "devil is in the details" regarding this statement [3–8], but a simple rule of thumb is that when water molecules, during the diffusion time, cannot exit a certain region due to physical barriers, the observed or "apparent" diffusion will appear smaller than in an unbounded medium of the same "solvent." Similarly, the direction of the gradient with respect to local tissue architecture such as white matter fiber tracts plays a significant role in the actual measurement. This latter feature is the basis of diffusion tensor imaging (DTI) and related diffusion tensor tractography (DTT) in which intra- and intervoxel preferred directions of water molecule travel are inferred, respectively, from measurements along multiple diffusion sensitization gradient directions [9–12]. Ignoring these complications for now, key aspects of Eq. (1) which must be understood are that typical *b* factors accessible with clinical MRI scanners, employing reasonable echo times (TEs) in the 80- to 170-ms range, are in the 2 to 5000 s/mm^2 range with the primary limitation being T2-related signal loss when attempting to achieve higher *b* factors. Considerably larger *b* factors are available with gradient subsystems associated with small animal imaging scanners at even shorter echo times. Alternate sequence approaches, such as the stimulated echo sequence in which the timing delay Δ can be varied, introducing only T1 vs. T2 signal loss, might be considered for higher *b*-factor studies with clinical scanners [13]. However, the most common generation of diffusion decay curves in human brain to date have been made using spin echo-based sequence in the which the *b* factor is varied by changing the gradient amplitude g with fixed δ and Δ. Within the confines of these approaches, significant progress in documenting and assessing the nonmonoexponential nature of diffusion decay curves in human brain has been made, despite incomplete and/or unsatisfying interpretations.

2. Essential experimental facts regarding brain water diffusion decay curves

Figs. 1 and 2 show some of the first results reported by our group [14] in human brain in vivo in which nonmonoexponential behavior was observed as a significant curvature in the ln *S* vs. *b* curves (Fig. 2). Generating similar plots of ln *S* vs. *b* in simple liquid phantoms of water, ethanol and isopropanol, always a good control experiment when assessing data over extended *b*-factor ranges, reveals only straight line diffusion decays into baseline noise on semi-log plots [14,15]. The brain diffusion decay curves in Fig. 2 display what can be characterized as a fast decay in the lower *b*-factor range and a slower decay at higher *b* factors. It must be noted that this phenomenon is distinctly different from much earlier discussions regarding a "perfusion" component potentially responsible for a very fast, and complex, decay in the *b*-factor range below 100 s/mm^2 [16–19], a subject we have reviewed previously [20].

The solid lines in Fig. 2 associated with the cortical gray matter and internal capsule diffusion decay curves are least squares best fits to our favorite function, the biexponential decay function

$$S=A\exp(-bD_A)+B\exp(-bD_B) \quad (2)$$

where *A* and *B* are the amplitudes of the fast and slow diffusion components, respectively, and D_A and D_B are their respective diffusion coefficients.

At this point, judgment is suspended on the suitability or appropriateness of the biexponential model and we review some facts that have been documented within the empirical framework which it affords in the assessment of human brain diffusion decay curves acquired using clinical scanners. The relative fraction of the fast diffusion component $A/(A+B)$ in adult human brain has been found to be generally higher than that of the slow component fraction and appears to be around 0.7 [14,15,21–35]. This statement must be qualified in that the fast fraction depends on the precise brain location and on the diffusion sensitization direction, particularly in white matter [21,27,28], as demonstrated in Fig. 3 for the internal capsule. Significantly larger fast fractions are observed in newborn vs. adult human brain, as shown in Fig. 4, indicating a significant developmental dependence of the overall shapes of the decay curves [22,23]. The size of the fast fraction was reported to be insensitive to TE as measured by Clark and LeBihan [21] over a TE range of 80 to 180 ms, though it would be of interest to explore smaller echo times, perhaps with STEAM-based approaches [13]. Our own work suggested that neither inversion pulses [29] nor magnetization transfer (MT) pulses [30] affected the basic properties of the biexponential decay, as demonstrated in Figs. 5 and 6. The quantitative analyses and conclusions from these latter two studies [29,30] suggest similar T1 and MT properties for any two water "compartments" that intrepid investigators may propose to represent the two diffusion components.

These are some of the most relevant facts that must be reconciled with any physical model proposed to describe the nonmonoexponential nature of brain water diffusion decay curves. Since they are facts based upon the delicate proposition of biexponential fitting to brain diffusion decay curves, we must return to considerations associated with the appropriateness of the biexponential fitting approach.

Biexponential fitting to experimental data, and/or multi-exponential fitting in general, is a well-recognized problem for which there is no dearth of pundits proclaiming how difficult it is to perform reliably. A somewhat extremist viewpoint along these lines [36] can be found in the textbook *Numerical Solutions That Work* by Princeton computer scientist Forman S. Acton who warns that Eq. (2), in which all four parameters are sought from experimentally noisy data, is extremely ill-conditioned AND that those who persist in attempting to fit experimental data to such an equation "… must be spanked or counselled. At the very least, keep them from obstructing Progress and the computer!" Despite these words of wisdom, several independent groups have "plowed on" with the dubious endeavor and have measured and fit both human [14,15,21–35] and animal [37–43] brain diffusion decay curves to biexponential functions with a reasonably high degree of consensus regarding the values for the free parameters of the biexponential, usually expressed in the form of three rather than four parameters with the use of normalized signal diffusion decay curves S/S_0, where $S_0=A+B$. The consensus among practitioners argues, at the very least, that biexponential fitting is a convenient empirical tool despite the multitude of criticisms that may arise from its use, including problematic physical interpretations (vide infra). This brings us to the final most obvious feature of the biexponential fit: it is often seen as implicitly supporting a physical model in which brain tissue voxels contain two different water compartments with different diffusion coefficients having relative water compartment sizes of $A/(A+B)$ and $B/(A+B)$. The complications that this assumption begets, and the alternative interpretations that have arisen as a result, largely form the basis of the Ruminations section below. Before launching into these ruminations, however, we recognize that even as an empirical tool, the biexponential function is not everyone's favorite function. At least three other, model free, few parameter fits have been proposed to capture the essential curvature displayed by brain diffusion decay curves. These are the "stretched-exponential model" [43], the "kurtosis model" [32] and the "statistical model" [33], as now discussed.

The stretched-exponential function proposed by Bennett et al. [43] reads:

$$S = S_o \exp[(-bD)^{\alpha}] \quad (3)$$

where D and α are the two free parameters for normalized, S/S_o, fits to experimental decay curves and α, taking on values from 0 to 1, is referred to as the "stretching parameter." Bennett et al. [43] made a statistical comparison of the quality of fits of biexponential vs. stretched exponential functions to rat brain diffusion decay data and concluded that "20% of the voxels were better fit to the stretched-exponential model than to a biexponential model, even though the latter had one more adjustable parameter." This statement may also be interpreted as meaning that 80% of the voxels were better suited to biexponential as opposed to stretched-exponential functions, a number that probably would have been even higher if the authors had not limited their study to cerebral cortex voxels and had sampled white matter as well [43].

The "kurtosis model" discussed by Kiselev et al. [32] is described as a Taylor, or "cumulative," expansion of the logarithm of the signal with respect to b and truncated at the second term. It reads:

$$\ln S = \ln S_o - bD + (KD^2/6)b^2 + \ldots . \quad (4)$$

For normalized decays S/S_o, Eq. (4) provides a two-parameter fit for D and the "kurtosis excess" factor K, a measure of the "peakedness of a distribution." Experimental human diffusion decay curves in vivo were collected in gray matter, white matter, cerebrospinal fluid (CSF) and voxels assumed to contain gray matter and CSF from partial volume effects within the 2×2×3-mm^3 voxel volumes. A rather limited range of b factors from 50 to 2500 s/mm^2 were sampled, and an F-test was performed to determine whether the improved χ^2 values obtained from biexponential vs. kurtosis model fits were statistically significant. The authors concluded that, in regions of pure gray matter, the biexponential fit with its additional free parameter was "superfluous," although white matter and partially volume averaged CSF/gray matter fared better with the biexponential model, albeit further studies of the diffusion directional dependence in white matter were deemed necessary [32]. A mysterious "radius of convergence" for the b factor, obtained by setting Eq. (1) to 0 and solving for b (an imaginary b, of course), is introduced such that if b is less than this critical radius (only known by first determining the biexponential parameters), then the truncated kurtosis model should rival the full biexponential fit with its additional free parameter. In our view, the article by Kiselev et al. [32], despite its provocative title and curious mathematics, does not provide a very strong incentive to abandon biexponential fits in favor of a second-order polynomial. Particularly as only a limited range of b values under 2500 s/mm^2 were sampled, the biexponential fit apparently fared better in most brain voxels, and, finally, our own results in gray matter — with specific suppression of CSF using an inversion recovery approach — yielded high-quality biexponential decay curves [25].

Finally, another two-parameter competitor to the three-parameter biexponential fits was proposed by Yablonskiy et al. [33] who assumed a Gaussian distribution of diffusion coefficients $P(D)$, limited to positive values and centered around a single apparent diffusion coefficient (ADC) and endowed with a distribution width of σ. Thus for $D>0$, we have

$$P(D) = A\exp[-(D - \mathrm{ADC})^2/2\sigma^2] \quad (5)$$

where A is a normalization constant, not a free parameter. The signal S is obtained by integrating Eq. (5) over all positive D values and obtaining, for normalized decay curves, the following expression

$$S/S_0 = \left\{[1+\Phi(\mathrm{ADC}/\sigma\sqrt{2} - b\sigma/\sqrt{2})]/[1+\Phi(\mathrm{ADC}/\sigma\sqrt{2})]\right\}\exp(-b\mathrm{ADC}+b^2\sigma^2/2). \quad (6)$$

In this expression, Φ is the error, or erf, function numerically tabulated in commercially available numerical software packages. Reasonable fits using Eq. (6) as applied to experimentally obtained brain diffusion decay curves from human volunteers were obtained with ADC values around 0.9 $\mu m^2/ms$ and σ values around 0.3 $\mu m^2/ms$. No rigorous statistical comparison such as an F-test was performed to determine whether the statistical approach was equivalent to or better than biexponential fitting. It seems likely, however, that with one less parameter than the biexponential model, conclusions similar to the kurtosis model would have been reached, particularly in light of the limited b-factor range (b<2250 s/mm^2) employed in the study [33].

It is always prudent, in the interest of parsimony, to utilize functions with the minimal number of free parameters when performing empirical fits to experimental data. In this light, the two-parameter models just described may be useful for some brain diffusion decay curves particularly when the b-factor range is not extended beyond 2500 s/mm^2 or so. However, at the risk of being spanked [36], we suggest that the three-parameter biexponential function of Eq. (2) remains the best option for empirical fits to brain diffusion signal decay curves over extended b-factor ranges and may itself be found lacking when this range is extended even further, as suggested by early animal work from Pfeuffer et al. [41]. We now turn from empiricism to interpretation by reviewing some of the physical models recently proposed to help understand the nature of the nonmonexponentiality of brain signal diffusion decay curves.

3. Ruminations: biophysical modeling of brain water diffusion decay curves

As noted above, the fast diffusion component fraction $A/(A+B)$ in adult human brain matter appears to be on the order of 0.7, depending on the specific brain region sampled and, especially in white matter, on the direction of the diffusion sensitization gradient [14,15,21–25]. A persistent [44] and possibly erroneous [45] dogma, largely associated with ruminations regarding ischemia, is that the intracellular diffusion coefficient of water is smaller than the extracellular diffusion coefficient of water due to fewer restrictions, hydration binding sites, etc., in the latter. This has led to some speculation that the slow diffusion component of a biexponential fit may represent the intracellular water compartment and the fast diffusion component may represent the extracellular water compartment. Indeed, studies of model systems such as cell cultures [46,47], red blood cell [48] and/or erythrocyte ghost preparations [49] have utilized this concept gainfully. Schwarcz et al. [48] demonstrated, however, that even packed red blood cells with negligible extracellular space display biexponential diffusion decay curves with a fast diffusion component fraction $A/(A+B)$ of around 0.63, similar to brain diffusion decay curves. An equally large impediment to a direct interpretation of the fast and slow diffusion components as extra- and intracellular water compartments arises from the fact that the intracellular water fraction in typical brain tissue is around 0.8 with a corresponding extracellular water fraction around 0.2 [50,51]. Thus, the fast and slow fraction of the typical diffusion decay curves of 0.7 and 0.3 are approximately the reverse of what one would expect, a feature pointed out by Niendorf et al. [37] in one of the earliest articles documenting biexponential diffusion decay curves in rat brain.

Attempts to salvage an intracellular/extracellular interpretation for the slow and fast diffusion components must introduce a model in which the apparent volume fractions of the two

components are reconciled with their known relative sizes. One simple possibility is that the T2 values within the compartments are dissimilar so that by the time the diffusion-weighted images are generated, at TE values typically above 65 ms, respective T2 weightings of the compartments have altered the apparent volume fractions from their true sizes. Arguing against such an easy way out is the fact that the most detailed measurements of the transverse relaxation in brain tissue, as carried out by MacKay et al. [52–54], have generally interpreted brain parenchymal T2 decay curves (ln *S* vs. echo time in this case) as reflecting a major T2 component (50 ms<T2<120 ms) arising from both intra- and extracellular water and, in white matter, a smaller, short T2 component (T2<30 ms) arising from myelin-associated water. The myelin-associated water, with its short T2, would be expected to play no role in diffusion measurements at high *b* factors due to the long echo times employed. More critically, no obvious distinction between intra- and extracellular water T2 values has been inferred from detailed brain parenchymal T2 measurements to date, making a T2 explanation for the paradoxical reversal of the relative amplitudes of intra/extracellular water volumes inferred from diffusion signal decay curves problematic.

Another feature of a thorough model that might "save the day" for the intracellular/extracellular compartmentation interpretation is water exchange between the two compartments through semi-permeable cellular membranes during the course of the measurement. Such an exchange could serve to alter the apparent volume fractions, and diffusion coefficients, of the two diffusion components from their true physiological values. Indeed, in our first article reporting biexponential diffusion decay curves in human brain [14], we utilized the so-called Karger equations [55] to simulate decay curves when exchange between two compartments with volume fractions similar to intra- and extracellular water volume fractions is turned on. We found that for exchange rates of 10 Hz, suitable reproductions of the experimental data were possible. An unsatisfying feature of the approach was that the Karger equations, per se, were derived for the situation of small δ/Δ ratios that, for clinical scanners at high *b* factors, is simply not achieved and represents a theoretical problem which has yet to be addressed adequately. Furthermore, an uncomfortably high extracellular diffusion coefficient of 4.4 $\mu m^2/ms$ was required to mimic the experimental results when forcing physiologically realistic intra- and extracellular volume fractions into the model [14].

A more recent attempt to apply the intracellular/extracellular model to gray matter nonmonoexponential diffusion decay curves introduces a seven-parameter model with (a) water exchange between compartments, (b) distinct T2 values within each compartment and (c) the effects of restricted diffusion within the confines of the intracellular space assumed to consist of prolate spheroids [34]. The short axis of the prolate spheroidal cells was included as one of the seven fitting parameters determining the intrinsic, intracellular diffusion coefficient from an approximate series formula derived decades ago for diffusion perpendicular to parallel plates [3,56]. Given that a biexponential fit is effectively a three-parameter fit which compliments the experimental data quite adequately, it is unsurprising that the seven-parameter model proposed by Vestergaard-Poulsen et al. [34] accommodated experimental gray matter diffusion decay curves nicely. Furthermore, physiologically reasonable ranges for the model cell body short diameters around 8 μm and extracellular volume fractions around 0.19 were obtained. Best fit intrinsic intra- and extracellular diffusion coefficient model parameters were around 0.7 and 3.2 $\mu m^2/ms$, respectively, and the model supported a wide range of intracellular exchange rates but favored low values around 0.5 Hz for the intracellular exchange rate, corresponding to an intracellular mean water residence time of 2 s. The model also supported a wide range of extracellular T2 values between 50 and 425 ms, and inferred best fit intrinsic intracellular T2 values around 23 ms or below. But for the latter result, the model might be deemed a crowning success in providing a physiologically consistent basis for nonmonoexponential brain diffusion decay curves [34]. However, the very low intrinsic intracellular water T2 value of 23 ms remains unsupported from independent transverse

magnetization decay studies which have not been consistent with distinctly measurable "slow exchange" T2 values for intra- and extracellular water compartments in brain parenchyma [52–54]. Parenthetically, if 80% of the water in gray matter had a T2 value of 23 ms, as indicated by this model, then clinical T2-weighted brain imaging at all current field strengths would have to utilize shorter TE values than current values of 70 ms or more needed to "T2 weight" brain parenchyma.

Despite the shortcomings of the model proposed by Vestergaard-Poulsen et al. [34], an important feature of their approach is the appreciation that restricted diffusion effects caused by cell membranes most probably play a substantial role in the observed nonmonoexponential nature of brain diffusion decay curves. Indeed, for idealized restrictions, such as parallel plates stacked uniformly along the direction of the diffusion sensitization axis or diffusion perpendicular to the long axes of uniform diameter cylinders, theoretical formulations for diffusion decay curves have been available for some time [3,56] and, due to their complexity, have continued to evolve [8,57]. Theory predicts for idealized conditions sharp "diffraction" peaks in ln *S* vs. *B* curves, peaks as presented in simulations by Peled et al. [58] for uniform diameter cylinders and experimentally by Weng et al. [59] for diffusion along parallel plates consisting of a stack of closely placed transparencies. Specifically, Peled et al. [58] convincingly demonstrated how diffusion decay curves as measured perpendicular to an ensemble of cylinders with a distribution of radii approximating that found in frog sciatic nerve readily resembled the "biexponential" brain diffusion decay curves reported experimentally [14,15]. The moral of this lesson is that it is probably prudent to consider "restricted diffusion" effects, with all their challenging complications from an analytical perspective, in any comprehensive approach to understanding nonmonoexponential diffusion decay curves.

An insightful model incorporating elements of both camps — water compartmentation and geometrical aspects of restricted diffusion — to model nonmonoexponetial diffusion decay curves was proposed recently by Jespersen et al. [35]. The model does not invoke different compartmental T2 values nor does it explicitly consider exchange between water compartments but assumes that neurons, dendrites and axons supply the main sources of water restriction and compartmentation. These neuronal processes are represented as an ensemble of impermeable cylinders characterized by their local voxel density and an orientational distribution function with respect to the direction of the diffusion sensitization direction. The diffusion signal decay is taken to be composed of two distinct decays, one from water within the extracellular space and noncylindrical cells, such as glial cells, and another, more complex signal, from the dendrites and axons represented as an ensemble of tiny cylinders with a unique orientational distribution. The free parameters of the model include an effective diffusion coefficient D_{eff} for isotropic diffusion of water within the extracellular/noncylindrical cell matrix and diffusion coefficients D_{L} and D_{T} for diffusion along and perpendicular to the cylindrical moieties, respectively. The other model parameters are the "dendrite density" or "dendrite-associated water volume fraction" and the coefficients of a truncated spherical harmonic expansion of the orientational distribution function of the cylinders, $f(\theta,\phi)$, with respect to the diffusion gradient sensitization direction.

A thorough exploration of this rather complex model was performed [35] using a formalin-fixed newborn baboon brain sampled over a wide range of *b* factors from 880 to 15,000 s/mm^2 over 153 diffusion sensitization directions distributed over the unit sphere. With a truncated (l=2) spherical harmonic expansion of $f(\theta,\phi)$, a total of 10 free parameters allowed nice fits to simulated and experimental brain data with statistically demonstrated improvements over more common diffusion tensor or biexponential diffusion tensor models. A number of different brain regions representing white and gray matter were sampled in this study and all provided physiologically reasonable estimates of dendrite densities, from 0.53 to 0.74 fractions, D_{eff} values for the "noncylindrical" diffusion coefficient from 0.29 to 0.69 μm^2/ms, and D_{L}

and D_T values around 0.8 and 0.1 μm^2/ms, respectively. Of particular interest with this model is the potential for nonmonoexponential diffusion decay curves to provide cytoarchitectural parameters for brain imaging including dendrite density and cylindrical distribution functions, similar in nature to those derived from advanced diffusion tensor imaging algorithms [60,61], on a voxel-by-voxel basis. Such parameters may obviously be of value in fundamental studies of neurodegenerative processes and brain development. As the authors suggest, the model represents a "reasonable compromise between reflecting the actual biological reality and physical and mathematical simplicity and tractability."

Before leaving the discussion of the model proposed by Jesperson et al. [35], it is instructive to consider decay curves which might arise from a simple isotropic distribution of cylinders with distinct values for longitudinal and transverse diffusion coefficients with $D_L > D_T$. In this case, the orientational distribution function is simply represented by the size of the solid angle with respect to the diffusion sensitization gradient direction. Similar concepts were previously utilized to describe "perfusion" effects of directed flow [16] in diffusion imaging but are adjusted now to accommodate the effects of unrestricted diffusion along (D_L) and restricted diffusion perpendicular (D_T) to the cylinders. Specifically, given that θ is the polar angle between the direction considered and the diffusion sensitization direction, sinθ dθ is the solid angle size representing the number of cylinders "pointing that way," then a direct application of the Jespersen et al. [35] formalism leads to a signal decay S with b factor given by

$$S = f\exp(-bD_{\text{eff}}) + (1-f)/2 \times \int_0^{\pi} \sin\theta \exp[-b(D_L\cos^2\theta + D_T\sin^2\theta)]\,d\theta \quad (7)$$

where f is the fraction of the noncylindrical, isotropic diffusion space. The argument in the exponential within the integral takes into account the different effective b factors associated with the gradient strengths $g\cos\theta$ and $g\sin\theta$, and the different effective diffusion coefficients D_L and D_T, along and perpendicular to each cylinder, respectively. The integral is readily resolved by using the relation $\sin^2\theta = 1 - \cos^2\theta$, Taylor expanding the resulting $\exp[-b(D_L - D_T)\cos^2\theta]$ term and performing the relevant, trivial, integrations over the 0 to π interval for each term. A series summation for the signal is thus obtained which reads:

$$S = f\exp(-bD_{\text{eff}}) + (1-f)\exp(-bD_T) \times \sum_{n=1}^{\infty} [-b(D_L - D_T)]^{(n-1)}/[(2n-1)(n-1)!]. \quad (8)$$

The sum converges rapidly for typical values of the dimensionless parameter $b(D_L - D_T)$, and simulated diffusion decay curves based on this expression are provided in Fig. 7 along with a generic biexponential function representative of experimentally obtained diffusion decay curves. It is significant to note from Fig. 7 that, even without an additional "noncylindrical" space, significant nonmonoexponentiality is introduced with just the simplest assumption of many small cylinders oriented isotropically with respect to the diffusion sensitization gradient. Further development of the Jespersen et al. [35] model to incorporate nonisotropic diffusion for extracellular water within white matter as well as T2 and exchange effects would certainly be of interest.

Finally, some form of compartmentation of water within and without cells, with or without specific geometrical considerations, has provided the basis of the models just reviewed. An interesting alternative has been proposed recently by Le Bihan [24] in which the water compartmentation responsible for the fast and slow diffusion components of the biexponential decay takes on a different form. Namely, it is argued that water in a structured state, affiliated with charge distributions at membrane surfaces and extending tens of nanometers on either side of the membrane surface, may account for the slow diffusion component. The fast diffusion

component would then arise from bulk tissue water within both intra- and extracellular compartments which is "in fast exchange with water hydration shells around proteins and macromolecules." The model is appealing in many respects, and rather convincing "back of the envelope" calculations are provided to account for the vexing 70%/30% split between fast and slow diffusion components which hampers any direct intra-/extracellular interpretation. Reasonable mechanisms for the effects of cell swelling and proliferation on diffusion decay curves, effects which have been observed experimentally [15,26], have been forwarded as basically more volume of water soaked membranes per voxel within the "wet mind." The concept of diffusion sensitization direction effects on the apparent volume fractions, also observed experimentally (c.f. Fig. 3 and Refs. [21,27,28]), is also addressed if only qualitatively [24]. The idea that the slow and fast diffusion components "… correspond to two differently structured water pools, rather than specific water compartments" [24] is certainly worthy of consideration. It is, however, difficult to understand how two such pools could have such different diffusion coefficients (factor of ~4) and yet apparently have such similar T2 values [21], T1 values [29] and magnetization transfer ratios [30] (Figs. 5 and 6). The apparent indifference or "insouciance" of the biexponential parameters to these inherent magnetic property weightings favors, in our view, geometrical or cytoarchitectural interpretations for the nonmonoexponential diffusion decay phenomenon as opposed to interpretations based on water compartmentation alone.

4. Conclusions

We have attempted to review the basic experimental facts and interpretations currently available regarding brain water diffusion decay curves as measured over extended but clinically accessible *b*-factor ranges. There is little doubt that further work remains to be done in understanding the nonmonoexponential nature of these decays and as such, despite the 10 years of effort, the field remains young and exciting from an intellectual curiosity perspective and from a potentially useful diagnostic perspective. Unreviewed in this monograph is the potential clinical exploitation of the nonmonoexponential nature of brain water diffusion decay curves. Clearly, any one of the few-parameter, parsimonious functions discussed above might serve as a basis for empirical tissue characterization in common brain pathologies and brain development [22,23]. Preliminary and interesting findings in brain tumors [26], as shown in Fig. 8, as well as stroke [15], multiple sclerosis [31] and vascular dementia [62] have been reported although it remains to be seen how useful the additional efforts needed to acquire and analyze detailed diffusion decay curves from the brain will be for either diagnosis or gauging response to therapy. Certainly, the value of such efforts will be enhanced with an improved understanding of the phenomenon, motivating further research in this area.

Acknowledgments

RVM thanks Bruno Maraviglia and his colleagues who have sponsored and supported the yearly workshop "Magnetic Resonance and Brain Function", in Erice, Sicily, where these "ruminations" have been offered.

Appendix A. An addendum for q-space

As a helpful reviewer noted about our original manuscript, we had successfully avoided any direct discussion of the "*q*-space" formalism despite its use by others studying the nonmonoexponential diffusion decay phenomenon [31,59,62–70]. We herein attempt to rectify this omission.

The basic *q*-space premise [63,64] relies upon a theoretical Fourier relationship between the diffusion signal decay S with the experimental parameter $q=\gamma g\delta/2\pi$, not b, and a probability function $P(\Delta,R)$ which represents the probability of finding a spin at distance R from its initial

position after a "diffusion time" Δ, in the short pulse gradient limit $\delta \ll \Delta$. Within the context of this idealized, isotropic diffusion incarnation, and with the understanding that the common practice of redefining the "diffusion time" as $\Delta - \delta/3 \equiv t_D$ for clinical studies where high *b* factors are only achieved with $\delta \sim \Delta$ is a problematic approximation worthy of serious theoretical considerations [71], it is possible to understand how the *q*-space formalism lends itself to the study of compartmentation. Let us do so within the framework of our now familiar biexponential equation for signal decay with *b* factor. For the standard spin-echo diffusion sequence, the relationship between *b* and *q* is simply $b = 4\pi^2 q^2 (\Delta - \delta/3) \equiv 4\pi^2 q^2 t_D$. With this relation, the biexponential of Eq. (2) may be recast in the following *q*-space friendly format

$$S(q, t_D) = A\exp(-4\pi^2 t_D q^2 D_A) + B\exp(-4\pi^2 t_D q^2 D_B), \quad \text{(A1)}$$

where we see that the biexponential signal decay with *b* is transformed into a bi-Gaussian function of *q*. Now of course, if one Fourier transforms Gaussians, new Gaussians are born. Let us do the math and find the inverse Fourier transform of Eq. (A1) by multiplying both sides by $\exp(-i2\pi qR)$ and then integrating over *q* from 0 to infinity, the latter limit being another idealized condition of course (hint: complete the square and use Cauchy theorem to be rigorous and get your "pies" right). We then obtain

$$I(R, t_D) = A/(4(\pi t_D D_A)^{1/2})\exp(-R^2/4t_D D_A) + B/(4(\pi t_D D_B)^{1/2})\exp(-R^2/4t_D D_B), \quad \text{(A2)}$$

another bi-Gaussian, by Golly, but one from which *q*-space practitioners can measure the halfwidths and then promulgate their findings in terms of the physical "dimensions "of the "compartments" being probed. This may be understood by examining, for example, the first term on the right of Eq. (A2) and pondering the physical meaning of the full halfwidth of this Gaussian, symmetric about $R=0$, and given analytically by $4(t_D D_A \ln 2)^{1/2} \approx 3.33\ (t_D D_A)^{1/2}$. We see that in the case of free, unrestricted, isotropic diffusion, this halfwidth would grow linearly with the experimental parameter $(t_D)^{1/2}$ [or $(\Delta)^{1/2}$ in the limit $\delta \ll \Delta$ limit]. However, restricted diffusion within "compartment A" means that the spins will begin to bump into the walls after sufficiently long t_D values and so the halfwidth will get stuck, or at least stop growing linearly with $(t_D)^{1/2}$. At such t_D values and beyond, the halfwidths measured from the *q*-space Gaussians may then be, guardedly, interpreted as the physical dimensions of compartments under observation, along the direction of the diffusion sensitization gradient applied.

Summarizing the steps to the *q*-space approach, we have (i) plot signal vs. *q*, (ii) Fourier transform over *q* and (iii) interpret the halfwidths of the resulting Gaussian(s) as reflective of the physical dimension(s) of the compartment under observation. Excellent examples of the *q*-space formalism applied to ex vivo data from isolated optic and sciatic nerves may be found in some recent work by Bar-Shir and Cohen [65] and also from Ronen and Kim [66], investigators who had the luxury of obeying the short pulse gradient approximation of $\delta \ll \Delta$ with the high field spectroscopic systems employed. The raw data (*S* vs. *q*) from both of these studies appears convincingly bi-Gaussian, and comparisons between *q*-space estimated physical dimensions and actual axon diameters are made and, at least for the optic nerves, validated [65,66]. In the clinical realm where the condition $\delta \ll \Delta$ does not generally hold, interpretations of *q*-space halfwidths as representative of actual physical dimensions are made but with less confidence in the underlying assumptions, the interpretations of the sizes obtained and, obviously, with less validation. For example, Assaf et al. [31,62] performed *q*-space analyses of human brain data acquired in vivo with clinical scanners using the above formalism and generated "*q*-space displacement" maps based on the bi-Gaussian halfwidths. In addition, "*q*-space probability" maps, calculated from the relative amplitudes of the bi-Gaussians and stated to reflect the probability of "zero displacement" during t_D were generated and displayed

as outputs of the *q*-space formalism. Thus it may appear as if exciting new information and insight can be gained from *q*-space analyses regarding water compartmentation and motion. A closer look, however, reveals that the parameters measured or mapped from the studies just mentioned are also directly available from the parameters A, D_A, B and D_B obtained from biexponential fits of signal decay with *b* factor as they are analytically linked to the bi-Gaussian amplitudes and halfwidths embodied in Eq. (A2). That is, deciding to do *q*-space analyses with bi-Gaussian fits is formally equivalent to doing biexponential "*b*-space" analyses. Though we do not know what punishment Acton [36] might recommend for attempting nonlinear bi-Gaussian fits, we do suspect that the problem is just as mathematically tractable or intractable as biexponential fitting and so subject to the same criticism.

To conclude, we have shown at least one formal equivalence between *q*-space analyses and the "*b*-space analyses" that have been the focus of our review. We have no doubt that the same litany of problems — effects of exchange, distribution of compartment sizes, "diffusion time" definitions, geometrical restriction considerations, etc. — that plague the interpretation of nonmonoexponential signal decays with *b* factor also plague signal "decays" with *q*-factor. The *q*-space formalism offers a cosmetically different view of the same problem and, we believe, adds no further insight or information.

References

1. Stejskal EO, Tanner JE. Spin diffusion measurements: spin echoes in the presence of a time-dependent field gradient. J Chem Phys 1965;42:288–292.
2. Le Bihan D, Breton E, Lallemand D, Grenier P, Cabanis E, Laval-Jeantet M. Imaging of intravoxel incoherent motions: application to diffusion and perfusion in neurologic disorders. Radiology 1986;161:401–407. [PubMed: 3763909]
3. Robertson B. Spin-echo decay of spins diffusing in a bounded region. Phys Rev 1966;151:273–277.
4. Tanner JE, Stejskal EO. Restricted self-diffusion in colloidal systems by the pulsed-gradient, spin-echo method. J Chem Phys 1968;49:1768–1777.
5. Mitra PP, Sen PN, Schwartz LM, Le Doussal P. Diffusion propagator as a probe of the structure of porous media. Phys Rev Lett 1992;68:3555–3558. [PubMed: 10045734]
6. Latour LL, Mitra PP, Kleinberg RL, Sotak CH. Time-dependent diffusion coefficient of fluids in porous media as a probe of surface-to-volume ratio. J Magn Reson A 1993;101:342–346.
7. Latour LL, Svoboda K, Mitra PP, Sotak CK. Time-dependent diffusion of water in a biological system. Proc Natl Acad Sci USA 1994;91:1229–1233. [PubMed: 8108392]
8. Callaghan PT. Pulsed-gradient spin-echo NMR for planar, cylindrical, and spherical pores under conditions of wall relaxation. J Magn Reson A 1995;113:53–59.
9. Basser PJ, Mattiello J, LeBihan D. MR diffusion tensor spectroscopy and imaging. Biophys J 1994;66:259–267. [PubMed: 8130344]
10. Pierpaoli C, Jezzard P, Basser PJ, Barnett A, Di Chiro G. Diffusion tensor imaging of the human brain. Radiology 1986;201:637–648. [PubMed: 8939209]
11. Basser PJ, Pajevic S, Pierpaoli C, Duda J, Aldroubi A. In vivo fiber tractography using DT-MRI data. Magn Reson Med 2000;44:625–632. [PubMed: 11025519]
12. Mulkern RV, Davis PE, Haker SJ, Estepar RJS, Panych LP, Maier SE, et al. Complimentary aspects of diffusion imaging and fMRI: Structure and function. Magn Reson Imaging 2006;24:463–474. [PubMed: 16677953]
13. Lehnert A, Machann J, Helms G, Claussen CD, Schick F. Diffusion characteristics of large molecules assessed by proton MRS on a whole-body MR system. Magn Reson Imaging 2004;22:39–46. [PubMed: 14972393]
14. Mulkern RV, Gudbjartsson H, Westin C-F, Zengingonul HP, Gartner W, Guttmann CR, et al. Multi-component apparent diffusion coefficients in human brain. NMR Biomed 1999;12:51–62. [PubMed: 10195330]

15. Brugieres P, Thomas P, Maraval A, Hosseini H, Combes C, Chafiq A, et al. Water diffusion compartmentation at high *b* values in ischemic brain. AJNR Am J Neuroradiol 2004;25:692–698. [PubMed: 15140706]
16. Ahn CB, Lee SY, Nalcioglu O, Cho ZH. The effects of random directional distributed flow in nuclear magnetic resonance imaging. Med Phys 1987;14:43–48. [PubMed: 3561335]
17. Harpen MD. Comments on "The effects of random directional distributed flow in nuclear magnetic resonance imaging". Med Phys 1987;14:1092. [PubMed: 3696077]
18. Cho ZH, Ahn CB. Reply to comments of Harpen. Med Phys 1987;14:1092–1093. [PubMed: 3696077]
19. Maki JH, MacFall JR, Johnson GA. The use of gradient flow compensation to separate diffusion and microcirculatory flow in MRI. Magn Reson Med 1991;17:95–107. [PubMed: 1712421]
20. Mulkern RV, Haker SJ, Maier SE. Complimentary aspects of diffusion imaging and fMRI: II. Elucidating contributions to the fMRI signal with diffusion sensitization. Magn Reson Imaging 2007;25:939–952. [PubMed: 17442520]
21. Clark CA, Le Bihan D. Water diffusion compartmentation and anisotropy at high *b* values in the human brain. Magn Reson Med 2000;44:852–859. [PubMed: 11108621]
22. Jones RA, Palasis S, Damien Grattan-Smith J. The evolution of the apparent diffusion coefficient in the pediatric brain at low and high diffusion weightings. J Magn Reson Imaging 2003;18:665–674. [PubMed: 14635151]
23. Mulkern RV, Vajapeyam S, Robertson RL, Caruso PA, Rivkin MJ, Maier SE. Biexponential apparent diffusion coefficient parametrization in adult vs. newborn brain. Magn Reson Imaging 2001;19:659–668. [PubMed: 11672624]
24. Le Bihan D. The "wet mind": water and functional neuroimaging. Phys Med Biol 2007;52:R57–R90. [PubMed: 17374909]
25. Maier SE, Mulkern RV. Biexponential analysis of diffusion related signal decay in normal human cortical and deep grey matter. Magn Reson Imaging 2008;26:897–904. [PubMed: 18467062]
26. Maier SE, Bogner P, Bajzik G, Mamata H, Mamata Y, Repa I, et al. Normal brain and brain tumor: multi-component apparent diffusion coefficient line scan imaging. Radiology 2001;219:842–849. [PubMed: 11376280]
27. Maier SE, Vajapeyam S, Mamata H, Westin CF, Jolesz FA, Mulkern RV. Biexponential diffusion tensor analysis of human brain diffusion data. Magn Reson Med 2004;51:321–330. [PubMed: 14755658]
28. Clark CA, Hedehus M, Moseley ME. In vivo mapping of the fast and slow diffusion tensors in human brain. Magn Reson Med 2002;47:623–628. [PubMed: 11948721]
29. Mulkern RV, Zengingonul HP, Robertson RL, Bogner P, Gudbjartsson H, Guttmann CRG, et al. Multi-component apparent diffusion coefficients in human brain: relationship to spin-lattice relaxation. Magn Reson Med 2000;44:292–300. [PubMed: 10918329]
30. Mulkern RV, Vajapeyam S, Haker SJ, Maier SE. Magnetization transfer studies of the fast and slow tissue water diffusion components in the human brain. NMR Biomed 2005;18:186–194. [PubMed: 15578729]
31. Assaf Y, Ben-Bashat D, Chapman J, Peled S, Biton IE, Kafri M, et al. High *b*-value *q*-space analyzed diffusion-weighted MRI: application to multiple sclerosis. Magn Reson Med 2002;47:115–126. [PubMed: 11754450]
32. Kiselev VG, Il'yasov KA. Is the "biexponential diffusion" biexponential? Magn Reson Med 2007;57:464–469. [PubMed: 17326171]
33. Yablonskiy DA, Bretthorst G, Ackerman J. Statistical model for diffusion attenuated MR signal. Magn Reson Med 2003;50:664–669. [PubMed: 14523949]
34. Vestergaard-Poulsen P, Hansen B, Ostergaard L, Jakobsen R. Micro-structural changes in ischemic cortical gray matter predicted by a model of diffusion weighted MRI. J Magn Reson Imaging 2007;26:529–540. [PubMed: 17685422]
35. Jespersen SN, Kroenke CD, Ostergard L, Ackerman JJH, Yablonskiy DA. Modeling dendrite density from magnetic resonance diffusion measurements. Neuroimage 2007;34:1473–1486. [PubMed: 17188901]
36. Acton, FS. Numerical methods that work. 2nd printing. Washington, DC: The Mathematical Association of America; 1990. 253 p.

37. Niendorf T, Dijkhuizen RM, Norris DG, van Lookeren CM, Nicolay K. Biexponential diffusion attenuation in various states of brain tissue: implications for diffusion-weighted imaging. Magn Reson Med 1996;36:847–857. [PubMed: 8946350]
38. Assaf Y, Cohen Y. Non-mono-exponential attenuation of water and *N*-acetyl aspartate signals due to diffusion in brain tissue. J Magn Reson 1998;131:69–85. [PubMed: 9533908]
39. Ronen I, Moeller S, Ugurbil K, Kim D-S. Investigation of multi-component diffusion in cat brain using a combined MTC-DWI approach. Magn Reson Imaging 2006;24:425–431. [PubMed: 16677949]
40. Ronen I, Moeller S, Ugurbil K, Kim D-S. Analysis of the distribution of diffusion coefficients in cat brain at 9.4 T using the inverse Laplace transform. Magn Reson Imaging 2006;24:61–68. [PubMed: 16410179]
41. Pfeuffer J, Provencher SW, Gruetter R. Water diffusion in rat brain in vivo as detected at very large *b*-values is multicompartmental. MAGMA 1999;8:98–108. [PubMed: 10456372]
42. Sehy JV, Ackerman JH, Neil JJ. Evidence that both fast and slow water ADC components arise from intracellular space. Magn Reson Med 2002;48:765–770. [PubMed: 12417990]
43. Bennett KM, Schmainda KM, Bennett R, Rowe DB, Lu H, Hyde JS. Characterization of continuously distributed cortical water diffusion rates with a stretched-exponential model. Magn Reson Med 2003;50:727–734. [PubMed: 14523958]
44. Van Gelderen P, de Vleeschouver MHM, Despres D, Pekar J, van Zijl PCM, Moonen CTW. Water diffusion and acute stroke. Magn Reson Med 1994;31:154–163. [PubMed: 8133751]
45. Duong TQ, Ackerman JJH, Ying HS, Neil JJ. Evaluation of extra- and intracellular diffusion in normal and globally ischemic rat brain via ^{19}F NMR. Magn Reson Med 1998;40:1–13. [PubMed: 9660547]
46. Pilatus U, Shim H, Artemov D, Davis D, van Zijl PCM, Glickson JD. Intracellular volume and apparent diffusion coefficients of perfused cancer cell cultures, as measured by NMR. Magn Reson Med 1997;37:825–832. [PubMed: 9178232]
47. Pfeuffer J, Floel U, Leibfritz D. Monitoring of cell volume and water exchange time in perfused cells by diffusion-weighted ^{1}H NMR spectroscopy. NMR Biomed 1998;11:11–18. [PubMed: 9608584]
48. Schwarcz A, Bogner P, Mric P, Correze J-L, Berente Z, Pal J, et al. The existence of biexponential signal decay in magnetic resonance diffusion-weighted imaging appears to be independent of compart-mentalization. Magn Reson Med 2004;51:278–285. [PubMed: 14755652]
49. Thelwall PE, Grant SC, Stanisz GJ, Blackband SJ. Human erythrocyte ghosts: exploring the origins of multiexponential water diffusion in a model biological tissue with magnetic resonance. Magn Reson Med 2002;48:649–657. [PubMed: 12353282]
50. Nicholson C, Sykova E. Extracellular space structure revealed by diffusion analysis. Trends Neurosci 1998;21:207–215. [PubMed: 9610885]
51. Dobbing J, Sands J. Quantitative growth and development of human brain. Arch Dis Child 1973;48:757–767. [PubMed: 4796010]
52. MacKay AL, Whittall KP, Adler J, Li DKB, Paty DW, Graeb D. In vivo visualization of myelin water in brain by magnetic resonance. Magn Reson Med 1994;31:673–677. [PubMed: 8057820]
53. Whittall K, MacKay AL, Graeb DA, Nugent RA, Li DKB, Paty DW. In-vivo measurements of T2 distributions and water contents in normal human brain. Magn Reson Med 1997;37:34–43. [PubMed: 8978630]
54. MacKay AL, Laule C, Vavasour I, Bjarnason T, Kolind S, Burkhard M. Insights into brain microstructure from the T2 distribution. Magn Reson Imag 2006;24:515–525.
55. Karger J. Principles and application of self-diffusion measurements by nuclear magnetic resonance. Adv Magn Reson 1988;12:1–89.
56. Tanner JE. Transient diffusion in a system partitioned by permeable barriers. Applications to NMR measurements with the pulsed field gradient. J Chem Phys 1978;69:1748.
57. Frohlich AF, Ostergaard L, Kiselev VG. Effect of impermeable boundaries on diffusion-attenuated MR signal. J Magn Reson 2006;179:223–233. [PubMed: 16406628]
58. Peled S, Cory DG, Raymond SA, Kirschner DA, Jolesz FA. Water diffusion, T2, and compartmentation in frog sciatic nerve. Magn Reson Med 1998;42:911–918. [PubMed: 10542350]

59. Weng J-C, Chen J-H, Kuo L-W, Wedeen VJ, Tseng W-YI. Maturation-dependent microstructure length scale in the corpus callosum of fixed rat brains by magnetic resonance diffusion-diffraction. Magn Reson Imaging 2007;25:78–86. [PubMed: 17222718]
60. Pasternak O, Assaf Y, Intrator N, Sochen N. Variational multiple-tensor fitting of fiber-ambiguous diffusion-weighted magnetic resonance imaging voxels. Magn Reson Imaging 2008;26:1133–1144. [PubMed: 18524529]
61. Anderson AW. Measurement of fiber orientation distributions using high angular resolution diffusion imaging. Magn Reson Med 2005;54:1194–1206. [PubMed: 16161109]
62. Assaf Y, Mayzel-Oreg O, Gigi A, Ben-Bashat D, Mordohovitch M, Verchovsky R, et al. High *b* value *q*-space-analyzed diffusion MRI in vascular dementia: a preliminary study. J Neurol Sci 2002;203–204:235–239.
63. Callaghan PT, MacGowan D, Packer KJ, Zelaya FO. High resolution *q*-space imaging in porous materials. J Magn Reson 1990;90:177–182.
64. Cory DG, Garroway AN. Measurement of translational displacement probabilities by NMR: an indicator of compartmentation. Magn Reson Med 1990;14:435–444. [PubMed: 2355827]
65. Bar-Shir A, Cohen Y. High *b*-value *q*-space diffusion MRS of nerves: structural information and comparison with histological evidence. NMR Biomed 2008;21:165–174. [PubMed: 17492659]
66. Ronen I, Kim D-S. Compartment specific *q*-space analysis of diffusion-weighted data from isolated rhesus optic and sciatic nerves. Magn Reson Imaging 2009;27:531–540. [PubMed: 18929454]
67. King MD, Houseman J, Gadian DG, Connelly A. Localized *q*-space imaging of the mouse brain. Magn Reson Med 1994;32:707–713. [PubMed: 7869892]
68. Cohen Y, Assaf Y. High *b*-value *q*-space analyzed diffusion-weighted MRS and MRI in neuronal tissue: a technical review. NMR Biomed 2002;15:516–542. [PubMed: 12489099]
69. Avram L, Assaf Y, Cohen Y. The effect of rotational angle and experimental parameters on the diffraction patterns and micro-structural information obtained from *q*-space diffusion NMR; implication for diffusion in white matter fibres. J Magn Reson 2004;169:30–38. [PubMed: 15183354]
70. Chin C-L, Wehrli FW, Fan Y, Hwang SN, Schwartz ED, Nissanov J, et al. Assessment of axonal fiber tract architecture in excised rat spinal cord by localized NMR *q*-space imaging: simulations and experimental studies. Magn Reson Med 2004;52:733–740. [PubMed: 15389948]
71. Mitra PP, Halperin BI. Effects of finite gradient-pulse widths in pulsed-field-gradient diffusion measurements. J Magn Reson A 1995;113:94–101.

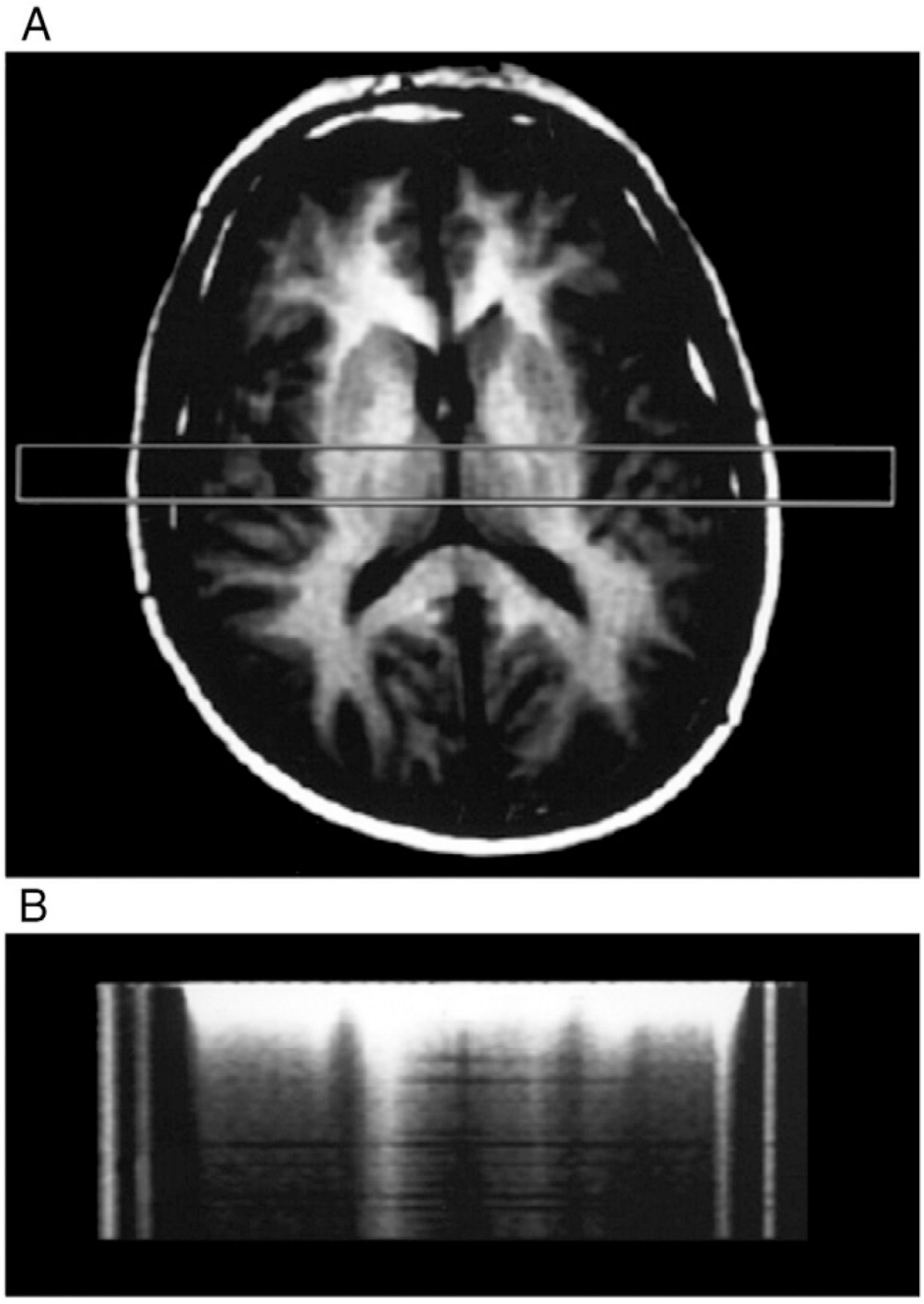

Fig. 1.

The horizontal column outlined in the image (A) was interrogated with 64 increasing values of diffusion weighting from 5 to 6000 s/mm^2, as shown from top to bottom in (B). Diffusion decay curves were extracted from locations along the column within the internal capsule, cortical gray matter and scalp lipid locations, and are plotted in Fig. 2 (reproduced from Ref. [14]).

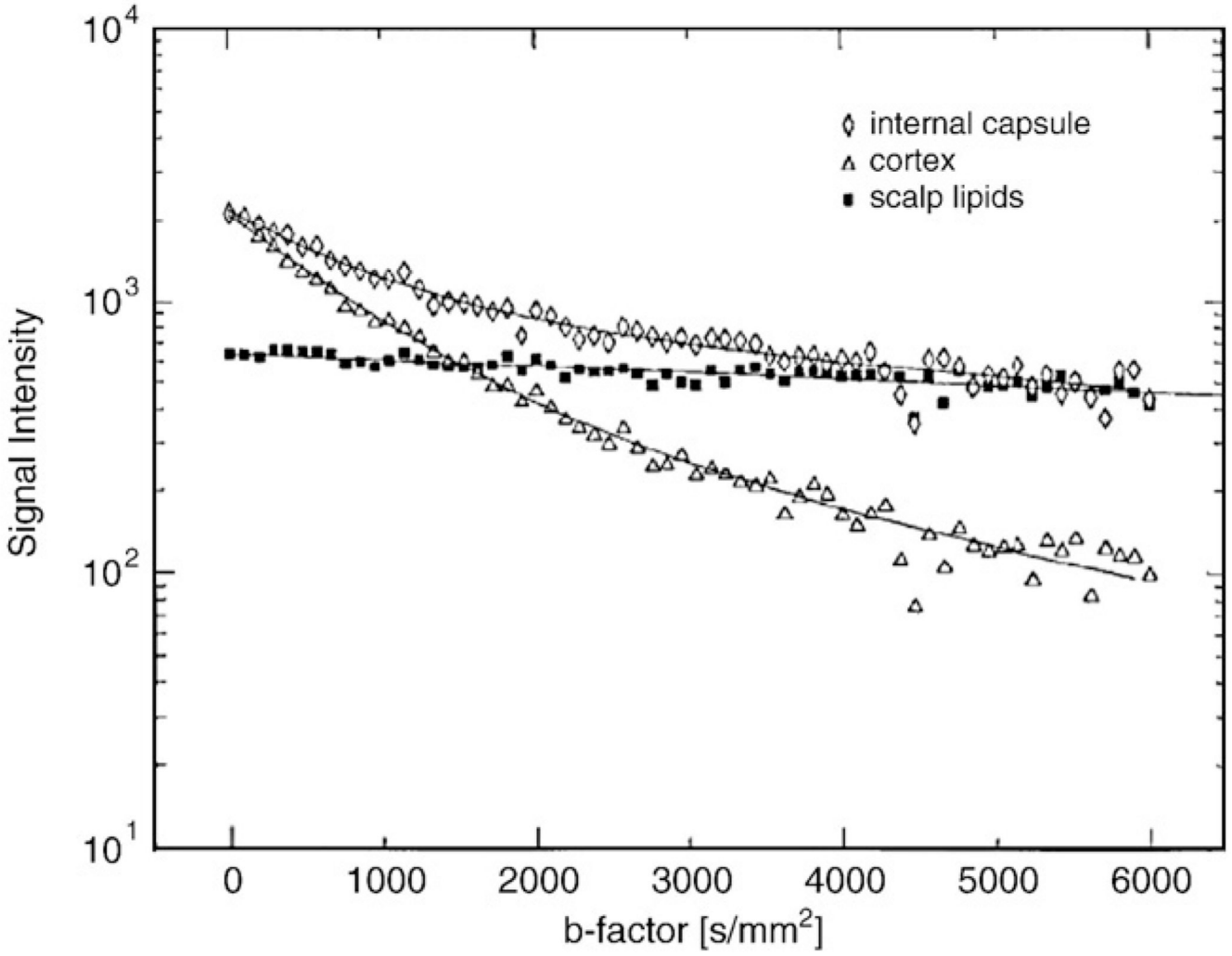

Fig. 2.

Semi-log plots of signal intensity vs. *b* factor, diffusion decay curves, as extracted from three locations (0.45 ml volumes) within the dataset of Fig. 1B. Note how the two diffusion decay curves from the brain locations in internal capsule and cortex show distinct curvature, indicating nonmonoexponential behavior which is well characterized with biexponential functions (solid lines). The scalp lipid signal diffusion decay curve has been fit with a mono-exponential function and displays an extremely low diffusion coefficient due to the high molecular weight of the triglycerides (reproduced from Ref. [14]).

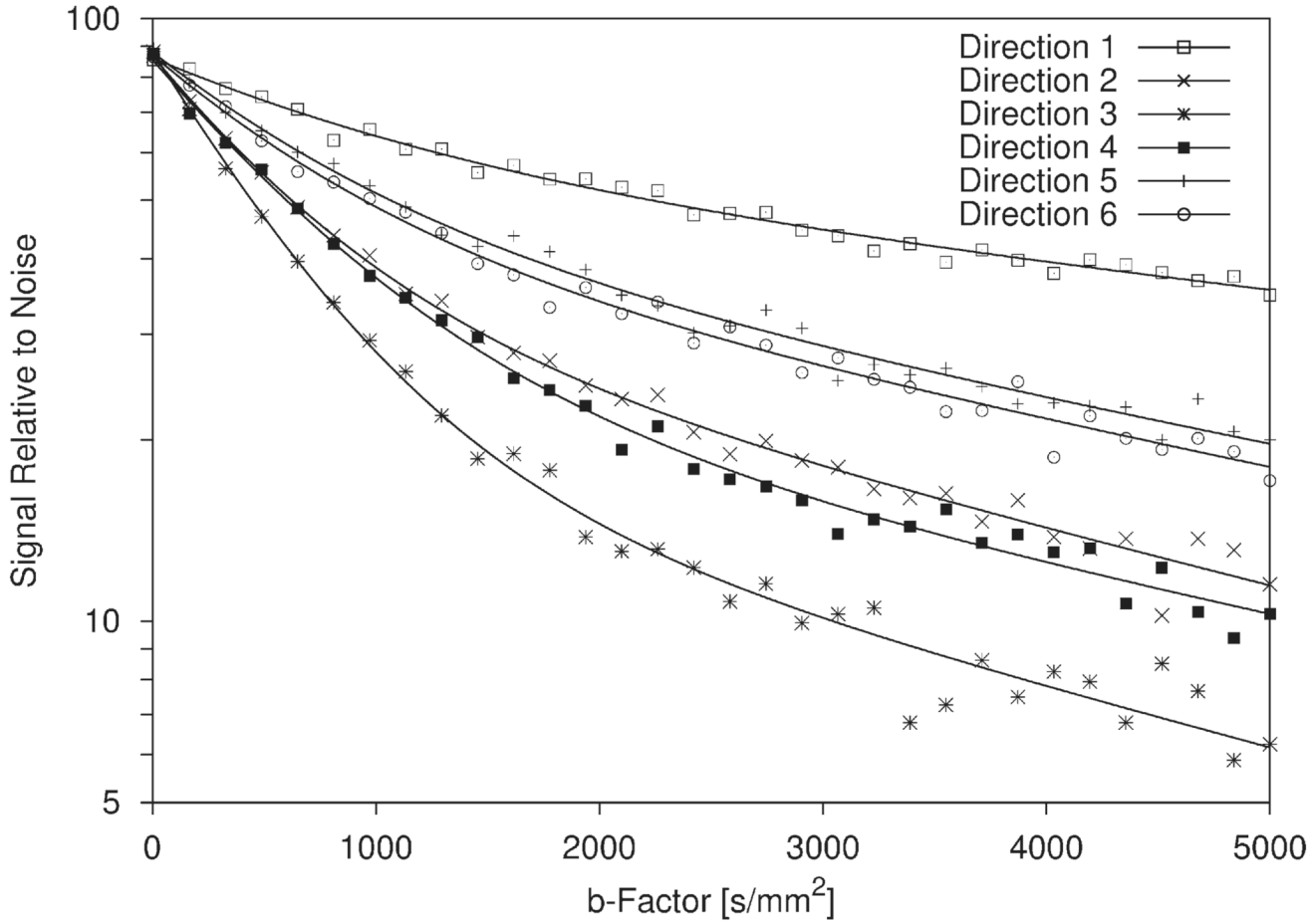

Fig. 3.

Diffusion decay curves from the internal capsule of a healthy adult volunteer as measured along six different diffusion sensitization directions (reproduced from Ref. [27]). The fibers in the internal capsule generally run along the *z*-direction (0,0,1), and the six directions displayed and labeled Directions 1–6 are (1,1,0), (0,1,1), (1,0,1), (0,1,−1), (1,−1,0), (−1,0,1). Note the apparent increase in the slow component size for Directions 1 and 5 where the diffusion sensitization gradient runs largely perpendicular to fibers in the internal capsule (reproduced from Ref. [27]).

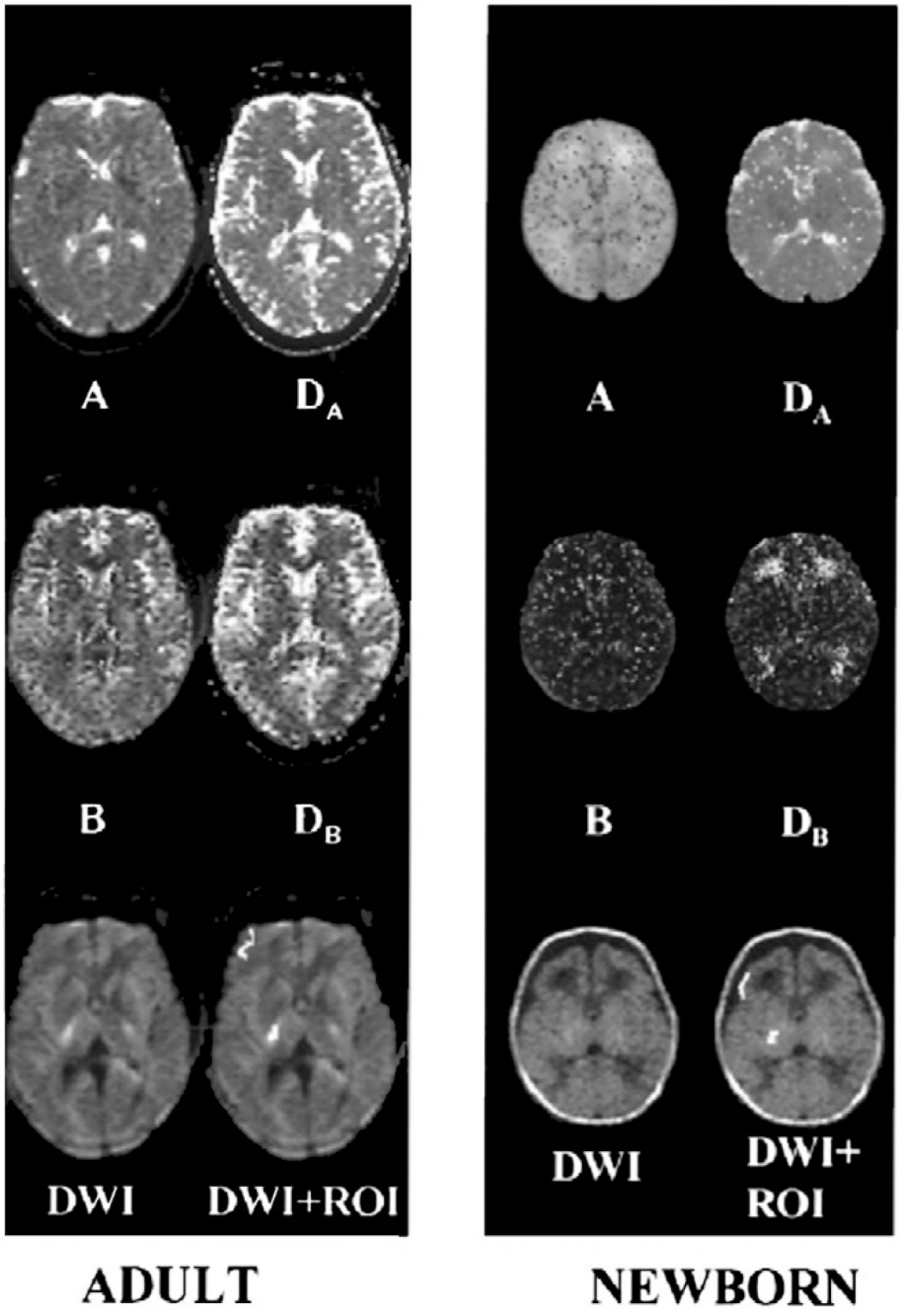

Fig. 4.

Parametric images of the biexponential parameters available from pixel-by-pixel fits of diffusion decay datasets in adult brain and newborn brain (reproduced from Ref. [23]). The amplitude of the fast diffusion component A is significantly higher in newborn brains which have only a small slow diffusion component amplitude B than in adult brains. ROI analyses of decay curves from the cortex and internal capsule (lower images) were used to quantify this observation as discussed in Ref. [23].

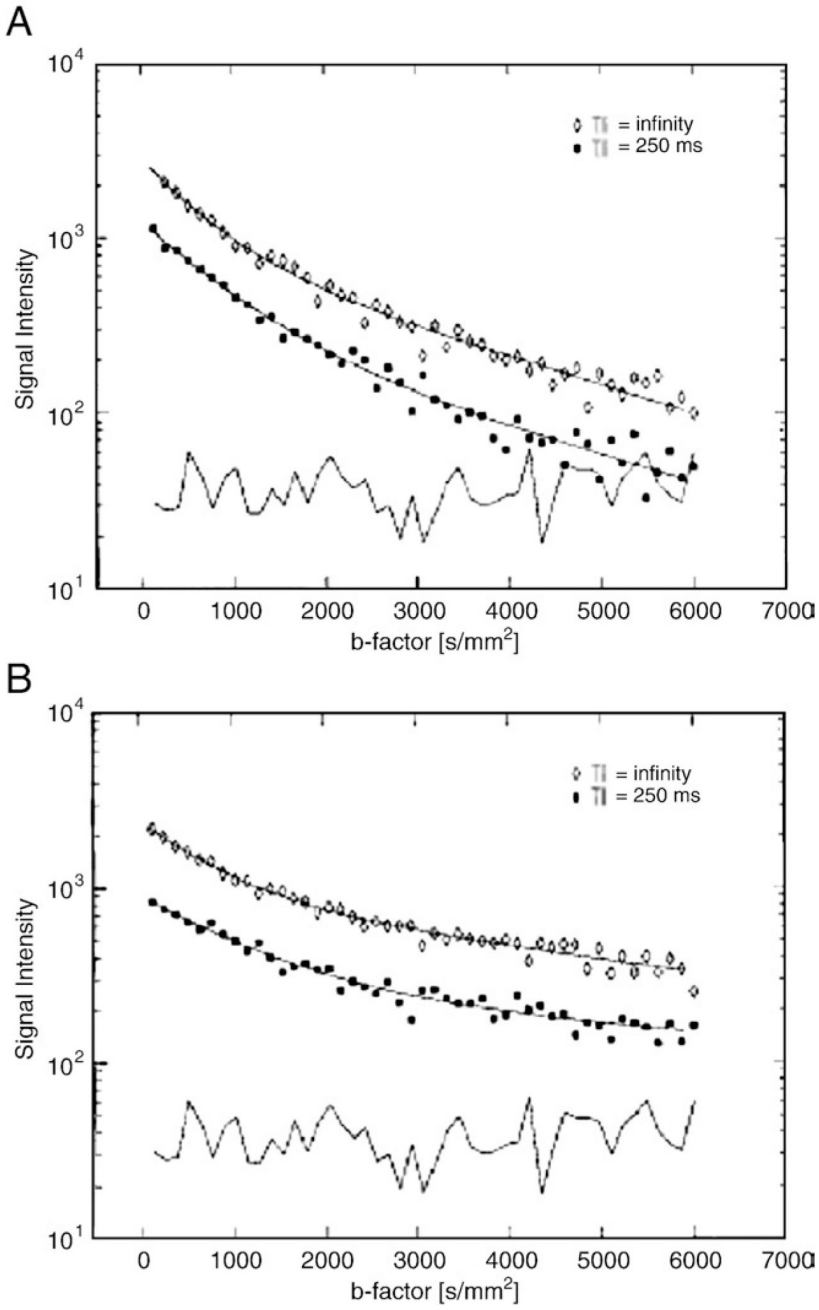

Fig. 5.

Diffusion decay curves from the cortex (A) and internal capsule (B) as acquired with an inversion pulse with an inversion time of 250 ms (solid squares) and without any inversion pulse (open diamonds). Noise values from air outside of the head at each *b* factor are shown along the bottom of each plot (solid line). Note how the inversion pulse has caused a significant decrease in signal intensity all along the decay curve but has not significantly altered the overall shape of the decay curves which, when characterized with biexponential functions, have similar fast and slow diffusion coefficients with no measurable change in the relative fraction of the slow vs. fast component amplitudes (reproduced from Ref. [29]).

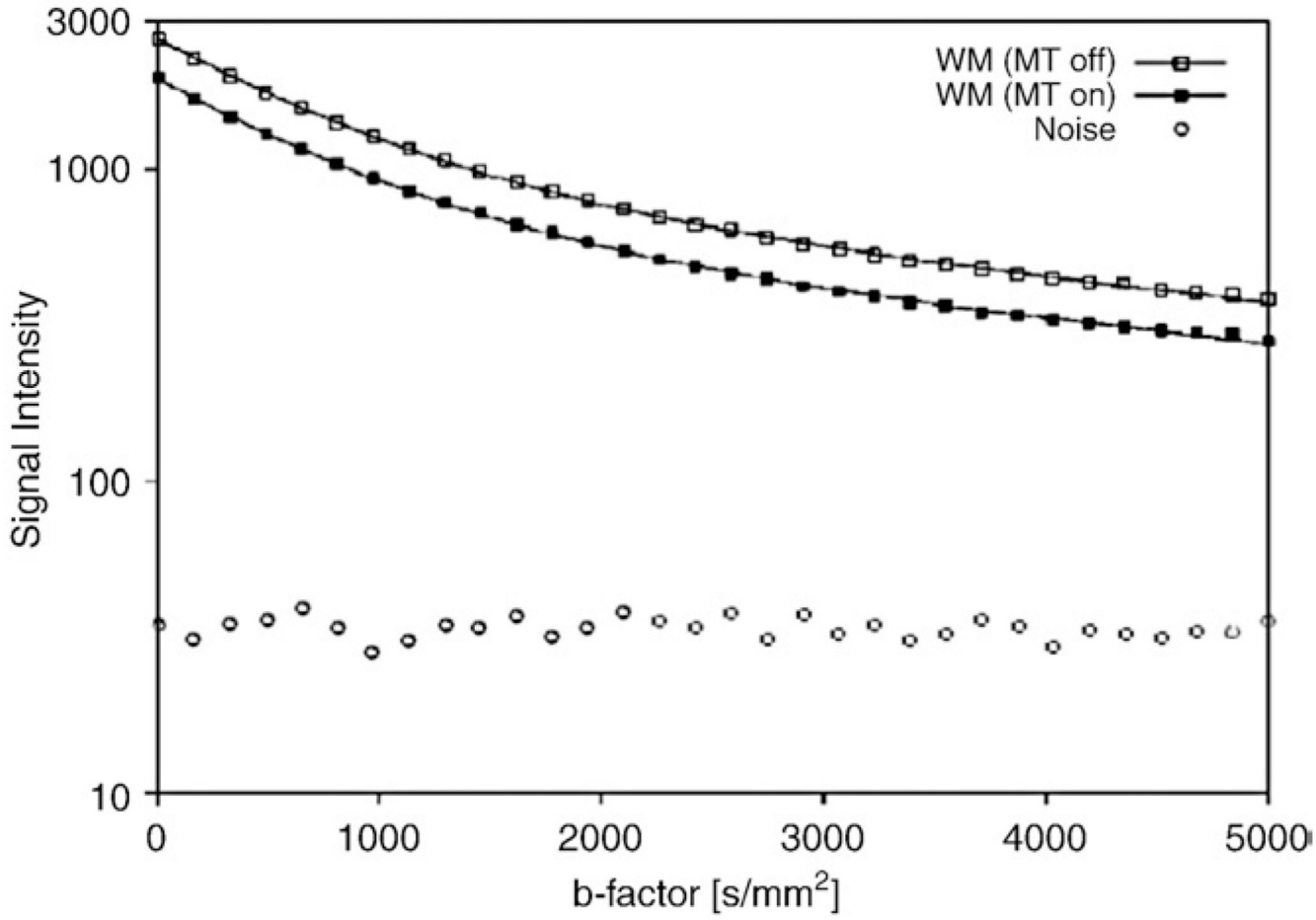

Fig. 6.

Diffusion decay curves from white matter volume as acquired with (solid squares) and without (open squares) a magnetization transfer (MT) pulse. Noise values from air outside the head are plotted for each *b* factor, taken from MT off data (circles). Note how the MT pulse causes a significant drop in signal intensity throughout the entire *b*-factor range but does not fundamentally alter the shape of the decay curve. Biexponential fits (solid lines) showed no measurable difference in fast and slow diffusion coefficients or relative fraction of the slow and fast component amplitudes between the MT condition and non-MT condition, similar to the T1-weighting results of Fig. 5 (reproduced from Ref. [30]).

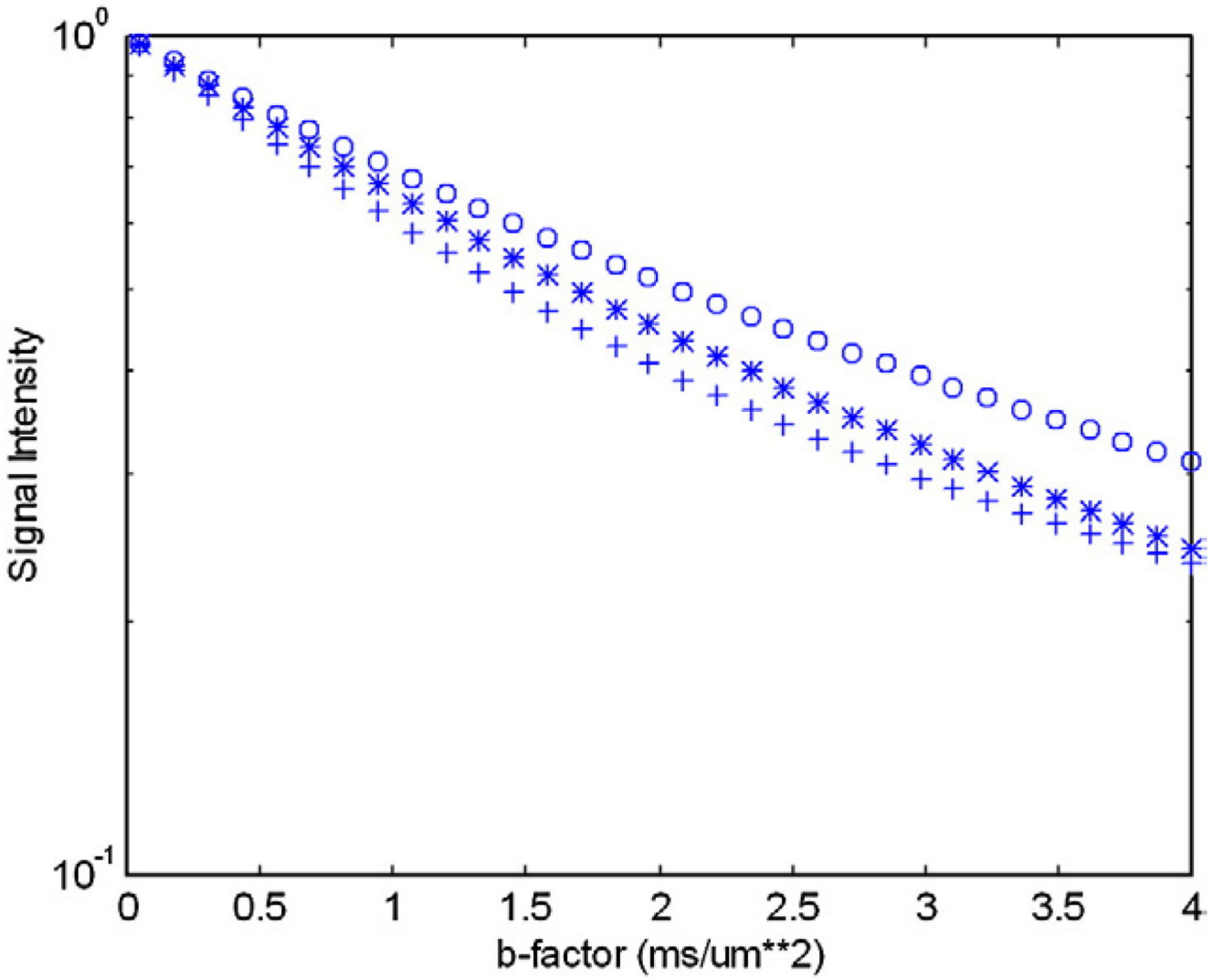

Fig. 7.

Decay curves from a generic biexponential function (crosses) with $A/(A+B)=0.7$ and D_A and D_B values of 0.75 and 0.1 μm^2/ms, respectively. The two other decay curves were generated using the cylindrical space model proposed by Jespersen et al. [35] but for an isotropic distribution of cylinders as averaged over all solid angles with respect to the diffusion sensitization directions with D_L and D_T values of 1 and 0.1 μm^2/ms, respectively, with (stars) and without (circles) a contribution from a noncylindrical space occupying 30% of the voxel with a D_{eff} of 0.6 μm^2/ms.

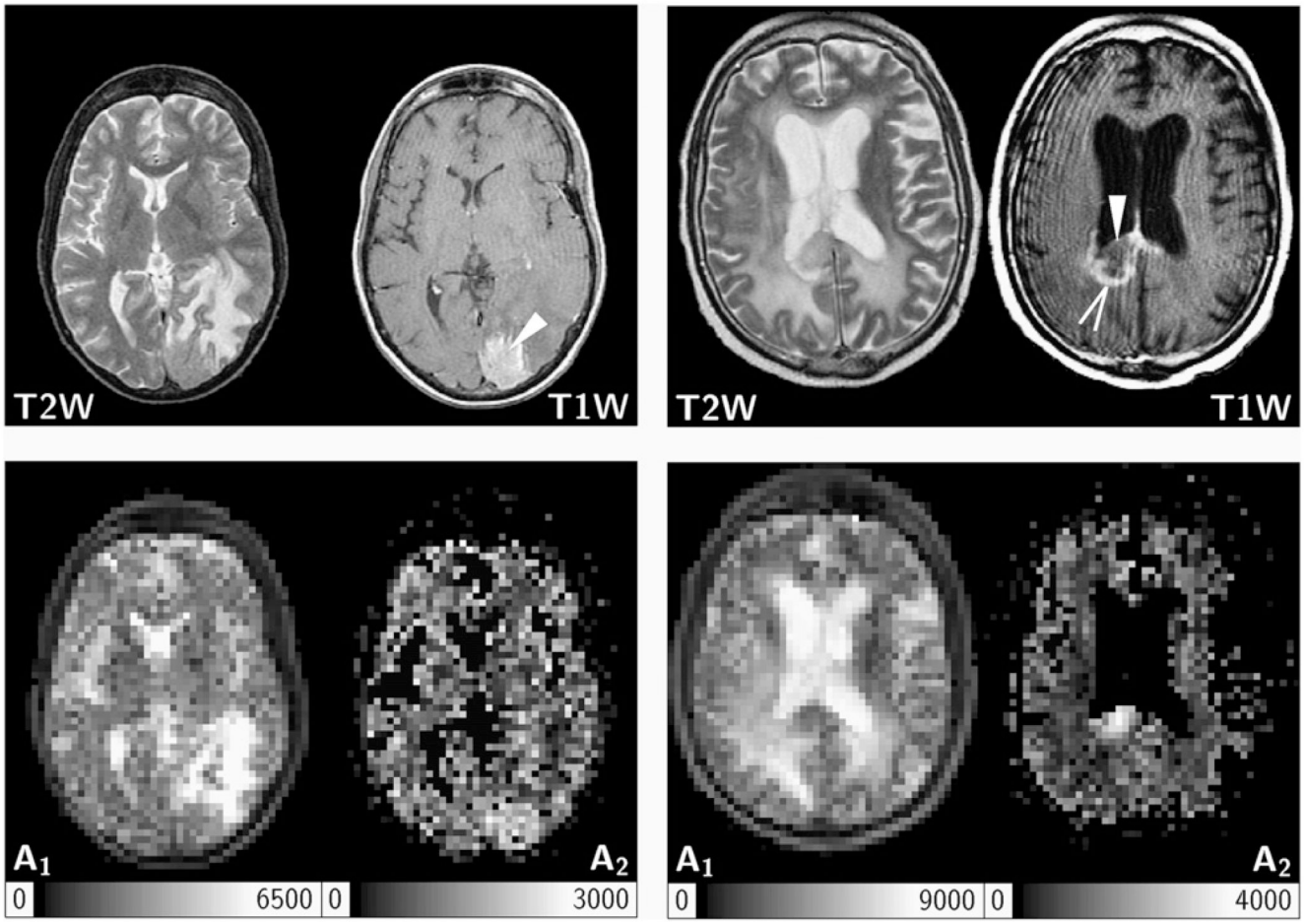

Fig. 8.

Two separate brain tumor patients with standard T2-weighted and post-Gd contrast T1-weighted imaging and high *b* diffusion imaging with subsequent postprocessing to yield biexponential-based parameter maps of the fast (A_1) and slow (A_2) diffusion component amplitudes (reproduced from Ref. [26] and using the notation there as opposed to that in the current text). For the patient on the left, there is an increase in the slow diffusion component fraction A_2 that corresponds to the region of Gd enhancement, in contrast to the patient on the right where the increase in A_2 lies within the rim of Gd enhancement. Edema, bright on T2W images in both patients, appears as an increase in the fast diffusion component fraction A_1.